Supramolecular hydrogels based on cellulose for sustained release of therapeutic substances with antimicrobial and wound healing properties

Article *in* Data in Brief · May 2020

DOI: 10.1016/j.dib.2020.105902

CITATIONS
0

READS
76

10 authors, including:

Oscar Javier Forero Doria
Universidad de Talca
29 PUBLICATIONS **118** CITATIONS
SEE PROFILE

Efraín Polo
Universidad de Talca
12 PUBLICATIONS **28** CITATIONS
SEE PROFILE

Adolfo Marican
Universidad de Talca
34 PUBLICATIONS **195** CITATIONS
SEE PROFILE

Luis Guzmán
Universidad de Talca
31 PUBLICATIONS **315** CITATIONS
SEE PROFILE

Carbohydrate Polymers 242 (2020) 116383

Contents lists available at ScienceDirect

Carbohydrate Polymers

journal homepage: www.elsevier.com/locate/carbpol

Supramolecular hydrogels based on cellulose for sustained release of therapeutic substances with antimicrobial and wound healing properties

Oscar Forero-Doria[a,1], Efrain Polo[a,1], Adolfo Marican[a,g], Luis Guzmán[b], Bernardo Venegas[c], Sekar Vijayakumar[d], Sergio Wehinger[b,e], Marcelo Guerrero[b], Jaime Gallego[f], Esteban F. Durán-Lara[g,h,*]

[a] Instituto de Química de Recursos Naturales, Universidad de Talca, Talca, 3460000, Maule, Chile
[b] Department of Clinical Biochemistry and Immunohematology, Faculty of Health Sciences, University of Talca, P.O. Box 747, Talca, 3460000, Maule, Chile
[c] Department of Stomatology, Faculty of Health Sciences, University of Talca, Talca, Chile
[d] Marine College, Shandong University, Weihai, 264209, PR China
[e] Center for Studies of Exercise, Metabolism and Cancer (CEMC), Universidad de Chile, Independencia, 8380000, Región Metropolitana, Chile
[f] Química de Recursos Energéticos y Medio Ambiente, Instituto de Química, Facultad de Ciencias Exactas y Naturales, Universidad de Antioquia UdeA, Calle 70 No. 52-21, Medellín, Colombia
[g] Bio & NanoMaterials Lab, Drug Delivery and Controlled Release, Universidad de Talca, Talca, 3460000, Maule, Chile
[h] Departamento de Microbiología, Facultad de Ciencias de la Salud, Universidad de Talca, Talca, 3460000, Maule, Chile

ARTICLE INFO

Keywords:
Sustained release
Cellulose
Hydrogel
Nanotube
Wound healing
Antibacterial activity

ABSTRACT

A multifaceted hydrogel-based formulation was reported. The hydrogel was prepared by crosslinking cellulose and substituted chalcone. Moreover, the formulation was conjugated with carbon nanotubes with the aim of increasing the loading amount of bioactive compounds such as allantoin, dexpanthenol, resveratrol and linezolid. The hydrogel formation was confirmed by swelling tests, FT-IR spectroscopy, thermogravimetric analysis and SEM. The hydrogel showed an improved release rate of therapeutic substances, exhibiting a simultaneous and coordinated release according to the chromatographic studies. The efficacy of drug release was confirmed by wound closure and *in vivo* wound healing studies that showed promising healing results. The antibacterial assays demonstrated that the sustained release of linezolid tends to be very effective. In conclusion, a multifaceted formulation based on carbon nanotube-containing cellulose-chalcone was developed that can potentially be utilized in treating complex wounds owing to its improved wound healing properties and prevention of potential infections.

1. Introduction

Wound management remains the main concern in clinical care due to the persistent incidence of traumatic injuries, the increasing prevalence of chronic wounds such as diabetic ulcers, varicose ulcers, and pressure sores, and aging populations that exhibit diminished wound healing capacity (Blacklow et al., 2019; Mihai, Dima, Dima, & Holban, 2019). Consequently, delayed wound healing leads to prolonged microbial infections that directly contribute to the chronic wound state.

The discovery and development of effective antimicrobial agents throughout the last century have led to a decrease in illness and deaths. However, the rampant usage of antibiotics and lack of new drug development by the pharmaceutical industry have made treating antibiotic resistance a difficult challenge. Consequently, infectious diseases caused by multidrug-resistant (MDR) microorganisms have become a threat to public health (Sefton, 2002; Ventola, 2015; Vijayakumar et al., 2019). For instance, strains of enterococcal MDR bacteria such as *Enterococcus faecium* have emerged as a leading cause of multidrug-resistant hospital-acquired infection. This bacterium causes antibiotic-resistant infection of the bloodstream, urinary tract, and surgical wounds (Adesida, Ezenta, Adagbada, Aladesokan, & Coker, 2017; Lebreton et al., 2013). Among the few available antibiotics that can treat bacterial resistance is linezolid. This antibiotic is effective in treating skin and soft tissue infections and exhibits effective inhibition against biofilm-embedded MRSA infections that are triggered by drug-resistant bacteria. (Reiter, Villa, Paim, de Oliveira, & d'Azevedo, 2013;

* Corresponding author at: Bio & NanoMaterials Lab, Drug Delivery and Controlled Release and Departamento de Microbiología, Facultad de Ciencias de la Salud, Universidad de Talca, Talca 3460000, Maule, Chile.
E-mail address: edura@utalca.cl (E.F. Durán-Lara).
[1] These authors contributed equally to this work.

https://doi.org/10.1016/j.carbpol.2020.116383
Received 21 January 2020; Received in revised form 24 April 2020; Accepted 24 April 2020
Available online 23 May 2020
0144-8617/

Yue et al., 2013).

Decades ago, several bioactive compounds with healing properties such as allantoin were reported. Allantoin is a natural compound and has shown multiple properties related to wound healing including hydrating and removing necrotic tissue, stimulating cell mitosis, and promoting epithelial stimulation, among others (Durmus, Yaman, & Can, 2012; Sowa et al., 2018). Another compound with similar properties is dexpanthenol. It acts as a moisturizer, stimulates fibroblast proliferation, accelerates re-epithelization, and has anti-inflammatory effects (Ebner, Heller, Rippke, & Tausch, 2002; Heise et al., 2012). Resveratrol is another natural compound that possesses antioxidant properties that can help the wound healing process while inhibiting inflammation (Liu, Tsai, Tsai, & Yu, 2015).

Despite considerable progress in the field, chronic wound healing has been a difficult challenge owing to bacterial drug resistance. To address this issue, a new generation of biomaterials has been developed such as metallic nanoparticles and bioactive dressings made from natural and synthetic polymers, among others (Mir et al., 2018; Murray, West, Cowin, & Farrugia, 2019). Among biomaterial wound dressings, hydrogels have also been investigated. Hydrogel applications include tissue engineering and drug delivery systems (Bertsch et al., 2019).

Hydrogels can be of natural and/or synthetic origin, ranging from natural proteins and carbohydrates to synthetic polymers (Capanema et al., 2018; Valdés et al., 2018; Wu et al., 2018). Hydrogels based on cellulose have recently received special attention because it is an abundantly available biomaterial with tunable properties and can be applied to systems with enormously diverse biochemical and biophysical environments (Hickey & Pelling, 2019). Cellulose has been widely studied due to its favorable properties including low cost, hydrophilicity, biocompatibility, biodegradability, and nontoxicity. At the structural level, the functional groups of cellulose can be modified easily, which makes it a promising starting material for the synthesis of biocompatible hydrogels (Fu, Qi, Ma, & Wan, 2019; Pan, Zhao, Li, & Cai, 2019). Although cellulose polymer itself does not exhibit any inherent antimicrobial activity, the high biocompatibility and functionality of this biopolymer allows antimicrobial applications of cellulose nanocomposites with various antimicrobial agents (Alavi, 2019; Wang, Pan, Cai, Guo, & Xiao, 2017). In this regard, cellulose-based hydrogels are considered useful biocompatible materials to be utilized in medical devices such as wound dressing hydrogels (Kabir et al., 2018; Mohamad, Loh, Fauzi, Ng, & Amin, 2019).

Multiwalled carbon nanotubes (MWCNTs) consist of numerous concentric graphene tubes and have diameters reaching 100 nm. For many applications in the biomedical field, MWCNTs are oxidized in strong acid to create hydroxyl and carboxyl groups as the functional ends to which biomolecules or other nanomaterials can be coupled. Moreover, due to their tubular shape, MWCNTs offer a high surface area and are amenable for adsorption and/or conjugation of a wide variety of therapeutic drugs. These features make MWCNTs attractive platforms for the treatment of several diseases (Bottini et al., 2006; Herlem et al., 2019). Therefore, the purpose of this study was to develop a supramolecular hydrogel based on cellulose for the sustained release of therapeutic substances with antimicrobial and wound healing properties that can potentially be utilized in treating complex wounds.

2. Materials and methods

2.1. Materials

Microcrystalline cellulose (MCC) powder (Catalog Number 11365, Avicel PH-101) was obtained from Merck (Darmstadt, Germany). $NaHCO_3$, acetonitrile (HPLC grade), allantoin, dexpanthenol, resveratrol, and linezolid analytical standards were purchased from Sigma-Aldrich (St. Louis, MO, USA). MCC, dialysis tubing (3.5 K MWCO, 22 mm), HCl and methanol (HPLC grade) K_2HPO4 and H_3PO4 were purchased from Merck (Darmstadt, Germany). All solutions were prepared using MilliQ water. *Enterococcus faecium* ATCC® 19434, brain heart infusion (BHI) agar, Luria-Bertani (LB), and peptone water were purchased from Merck (Darmstadt, Germany). Distilled water was utilized for the preparation of all the solutions in the antibacterial study. The mouse fibroblast cell line L929 (ATCC® CCL^{-1}™) was purchased from ATCC (Manassas, VA, USA). The cells were cultured in Dulbecco's modified Eagle's medium (DMEM, Gibco®, NY, USA) containing 10 % fetal bovine serum (FBS, Gibco®, NY, USA) and antibiotics (100 U penicillin and 100 U/mL streptomycin, Gibco®, NY, USA) under 5 % CO_2 at 37 °C. Cells were harvested after reaching confluence by using 0.05 % trypsin–EDTA (Gibco®, NY, USA).

2.2. Preparation of the microcrystalline cellulose (MCC) solution

In this procedure, a typical method was used to dissolve MCC in a NaOH/urea solution (Lin, Han, & Wang, 2018; Ye et al., 2016). First, 7 g of NaOH and 12 g of urea were dissolved in 76 g of ultrapure water. Then, 5 g of cellulose was added, obtaining a 5 wt% cellulose dispersion. The dispersion was frozen at −20 °C for 8 h and dissolved at room temperature with quick stirring. After defoaming by applying a centrifugation treatment at 2000 × g for 20 min at 25 °C, the obtained solution was saved at 4 °C for later use.

2.3. Preparation of MWCNTsCCH and loading of therapeutic substances

First, 1 g of the cellulose solution was mixed with chalcone (CH) (**3**) at 20 w/w %. The synthesis and characterization of CH are shown in the supporting information Section 1 and Figs. S1 and S2. The reaction mixture was continuously sonicated for 2 h (the temperature of the sonication bath ranged from 25 to 60 °C) according to the modified method from Cass, Knower, Pereeia, Holmes, and Hughes (2010). Then, a yellow viscous liquid corresponding to the crosslinked cellulose-chalcone prehydrogel was obtained. Second, as depicted in Table S1, MWCNTs (15 w/w%, MWCNTs-COOH, average size (diameter × length): 20–80 nm × 10–15 μm) were mixed with the prehydrogel and sonicated for 2 h at 50 °C (the MWCNT-COOH synthesis is shown in the supporting information, Section 2). Next, the homogenized black mixture (prehydrogel-MWCNTs) was dialyzed for 2 days. Then, the therapeutic substances (TSs) allantoin, dexpanthenol, resveratrol, and linezolid were added to the solution (Ávila-Salas et al., 2019). The resulting mixture was sonicated for 2 h at 50 °C until a homogenized solution was obtained. Finally, the mixture solution was placed in an oven at 45 °C overnight until the crosslinking was complete and the hydrogel film was formed. The obtained films were lyophilized and cut into 1.2 × 1.2 cm squares with a weight of ~ 400 mg. The final concentrations (w/w %) of allantoin, dexpanthenol, resveratrol, and linezolid were 3.4, 1.4, 1.4 and 1.4, respectively. Finally, the films were stored at 4 °C until they were analyzed. The formulation obtained by adding multiwalled carbon nanotubes-COOH with the crosslinked cellulose-chalcone hydrogel is abbreviated as MWCNTsCCH, and the same formulation loaded with therapeutic substances is named MWCNTsCCH-TS.

2.4. Equilibrium swelling ratio of MWCNTsCCH

The water uptake activity was calculated by the equilibrium swelling ratio (% ESR) at specific time intervals, according to the protocol of Marican, 2018. The MWCNTsCCH film was placed in phosphate-buffered saline (PBS) (pH 7.4) and acetate buffer (pH 4.0) at ~ 25 °C for 48 h until swelling equilibrium was reached. The weight of the wet sample [Ww (g)] was measured after cautiously removing surface moisture with absorbent paper. The weight of the dried sample [Wd (g)] was obtained after freeze-drying the prepared hydrogel. The ESR of the hydrogel samples was estimated according to the following equation (Eq. (1)):

$$\text{ESR}\ (\%) = \frac{W_w - W_d}{W_d} x\ 100\% \quad (1)$$

2.5. FT-IR measurement

The MWCNTsCCH sample was ground into small particles and freeze-dried for 24 h. The dried samples were analyzed in KBr disks by Fourier transform infrared spectroscopy (NEXUS 670 FT-IR, Thermo Nicolet, Madison, WI, USA). Samples for FT-IR measurements were prepared by grinding dry material into KBr in an agate mortar at a very low concentration of MWCNTs (0.03 wt%), MWCNTsCCH (0.02 wt%) and cellulose (1.0 wt%) (Smidt, Lechner, Schwanninger, Haberhauer, & Gerzabek, 2002). This very low concentration of MWCNTs and MWCNTsCCH is necessary to obtain clean FT-IR spectra due to the strong absorbance caused by CNTs, which are often unable to be distinguished from the background. The wavenumber range scanned was $4000-400\ cm^{-1}$; 32 scans of 2 cm^{-1} resolution were signal-averaged and stored. The films used in this work were sufficiently thin to obey the Beer-Lambert law.

2.6. Thermal analysis

The sample analyses of MWCNTs and MWCNTsCCH were performed in a thermogravimetric analyzer (STD 650 TA-235, TA Instruments). Approximately 3 mg of freeze-dried sample was placed into the instrument balance and heated at a constant heating rate of 10 °C min^{-1}. The heating was conducted from room temperature to 800 °C in N_2 or air as a reactive gas (with a mass flow of 50 mL min^{-1}.). The temperature was held at 800 °C for 30 min to allow the oxidation process to complete. Additionally, 50 mL min^{-1} N_2 was used as the protection gas in the electronic balance. Approximately 10 mg of the composite was placed into a platinum crucible for each analysis. The first region of the thermal analysis, from room temperature to 800 °C under an N_2 atmosphere, examines the thermolabile molecules or fragments that can be decomposed by simple heating of the samples, such as the functional groups over the carbon nanotubes. The second region, the oxidative process (under O_2), aims to observe the sample's oxidative resistance under extreme conditions, reactive gas (dynamic air atmosphere) and high temperature (800 °C).

2.7. Drug release kinetics from MWCNTsCCH-TS

The protocol was performed according to Ávila-Salas et al. (2019). A known mass of MWCNTsCCH-TS (400 mg of dry sample) was placed in a flask, and 5 mL of PBS (pH 7.4) was poured over the formulation as a release medium. The flask was moved to an orbital shaker incubator water bath (Farazteb, Iran) at 33.5 ± 0.1 °C (skin temperature) and shaken at 35 ± 2 rpm. After every time interval, the PBS was recovered and replaced with an equal volume to maintain sink conditions during all studies. The samples and controls were analyzed by a Perkin Elmer series 200 HPLC system (Norwalk, CT, USA) with a UV–vis detector. A YWG C-8 (250 mm × 4.6 mm i.d. × 10 μm) column was utilized for the sample analysis. A volume of 20 μL of eluent was injected into the equipment. The mobile phase utilized contained 20 mM K_2HPO_4 (pH 6.0, H_3PO_4)/methanol (90:10, v/v) in isocratic mode at a flow rate of 1.0 mL min^{-1}. The samples were monitored at 210 nm (allantoin and dexpanthenol) and 300 nm (resveratrol) by absorbance detection at 30 °C. For quantification of linezolid, a stock solution (3 mg/mL) was prepared in methanol and stored at −18 °C. Standard solutions of linezolid were prepared with PBS (pH 7.4) in the range of 0.01 mg L^{-1} to 50 mg L^{-1}. The chromatographic system consisted of a Perkin Elmer series 200 HPLC system (Norwalk, CT, USA) with a UV–vis detector and a C-18 Kromasil 100-5-C18 (250 mm × 4.6 mm i.d. × 5 μm) column. Fifty microliters of the sample was injected into the HPLC apparatus. Isocratic elution with methanol/water (50:50, v/v) at a constant flow rate of 1.0 mL min^{-1} was used as the mobile phase. The analytical wavelength was 254 nm at room temperature.

The release rate of MWCNTsCCH-TS was obtained by applying the concentration of released and loaded TSs to the following correlation (Eq. (2)):

$$\text{Cumulative TS release}\ (\%) = \text{Cumulative amount of TS released} \times \frac{100}{\text{Initial amount of TS}} \quad (2)$$

Drug release kinetics were carried out by applying different mathematical modeling drug-release equations, namely, zero-order (Eq. (3)), first-order (Eq. (4)), Hixson-Crowell (Eq. (5)), Higuchi (Eq. (6)), Korsmeyer–Peppas (Eq. (7)), and Peppas-Sahlin (Eq. (8)) equations (Dwivedi, Singh, & Dhillon, 2017; Owonubi, Aderibigbe, Mukwevho, Sadiku, & Ray, 2018):

$$Q_t/Q_0 = K_0 t, \quad (3)$$

$$\ln Q_t/Q_0 = K_1 t, \quad (4)$$

where Q_t is the amount of drug released at time t, and Q_0 is the original drug concentration in the hydrogel.

$$C_0^{1/3} - C_t^{1/3} = Kt, \quad (5)$$

where C_t is the amount of drug released in time *t*, C_0 is the initial amount of drug in the tablet, and K is the rate constant.

$$Q = Kt^{1/2} \quad (6)$$

where Q is the cumulative drug release, K is the Higuchi release constant, and t is the time

$$\frac{M_t}{M} = Kt^n, \quad (7)$$

where M_t/M is the cumulative drug release, K is the release constant, *t* is the time, and *n* is the release exponent.

$$\frac{M_t}{M\infty} = Kdt^n + Krt^{2n}, \quad (8)$$

where M_t and M_∞ are the absolute cumulative amounts of drug release at time t and at infinite time, respectively.

2.8. In vitro wound scratch characterizations

The L929 dermal fibroblast monolayer cell was scratched in a straight line using a sterile pipette tip to mimic an incision wound, as has been reported in several studies (Grimmig et al., 2019). Next, PBS was utilized to wash cells to eliminate cell fragments. Then, the cells were exposed to 500 μL of supernatant recovered (9, 24 and 48 h) from the solution that contained the formulation with and without TSs at certain time intervals at 37 °C. For the scratch wound assay using MWCNTsCCH-TS, scratch wound photographs were recorded at 0, 24 and 48 h. The scratch area was measured utilizing ImageJ software. Digital photographs were recorded by an inverted microscope (Olympus, Japan).

2.9. Animals and Maintenance Conditions and in vivo wound healing studies

The studies were performed in adult Sprague-Dawley rats (150–200 g) acquired from the animal facility from the Universidad de Talca. All the rats' care and experimental procedures were evaluated and approved by *Comité Institucional de Ética, Cuidado y Uso de Animales de Laboratorio* (CIECUAL) from the Universidad de Talca (Project identification code: 11170155; approval date of the committee: 17 December 2017). The rats were maintained under standard environmental conditions (22 ± 2 °C, relative humidity 75–80 %, 12 -h light cycle). The rats were weighed at the beginning and end of the experimental period.

Moreover, the intake of water and food was recorded. The animals were fed a standard diet manufactured by Champion (6.4 % moisture, 3.6 % lipids, 6.7 % protein, 7.3 ashes, 3.6 fibers, and 72.4 % carbohydrates). Rats were given *ad libitum* access to food and water; the beds were renewed three times a week. A record of changes in behavior or intake in each cage was updated daily by the personnel in charge. The method according to Ávila-Salas et al. (2019) was performed. In brief, the animals were distributed randomly into groups (4 animals per group). Before the beginning of the surgical process, all rats were sedated with isoflurane and anesthetized with a mixture of ketamine. With the drugged rats in the surgical position, depilation of the interscapular area was carried out with a hair clipper (Oster gold), and then, the area was washed with 0.25 % chlorhexidine soap. Afterward, one skin segment in the area of the back between the scapulae was removed; surgery was performed with a special scalpel. The biopsy diameter was approximately 1 cm. The open wounds were covered with to-be-studied wet film samples (MWCNTsCCH-TS and controls) and fixed with an elastic adhesive bandage. Two control groups in this trial were utilized: Madecassol™, a commercial product, and MWCNTsCCH (film dressing without therapeutic substances). Madecassol™ was applied daily until day 14. The total duration of the test was 14 days. However, on day 7, the MWCNTsCCH-TS and controls were removed to examine their adhesion, and the film dressing was not reapplied. From days 7–14, natural wound healing progression was monitored. The wound zones were inspected and photographed to measure the wound size reduction. The obtained results were expressed in terms of area and were represented by the zone closure of the wound. Differences in wound closure between the treated samples and controls were compared macroscopically. Once the wound healing experiments were completed, the rats were sacrificed by excess diethyl ether on day 14 after the surgery. The ratio of wound closure, which represents the percentage of wound reduction from the original wound size, was calculated using the following formula:

$$\text{Wound healing reduction (\%)} = \frac{\text{wound area day 0} - \text{wound area day 14}}{\text{wound area day 0}} \times 100 \quad (9)$$

The values are expressed as a percentage of the healed wounds ± SD.

2.10. Histological study

The method according to Ávila-Salas et al. (2019) was performed. Briefly, histological analysis was performed for microscopic observation of the wound closure zone. This analysis was based on comparing the wound healing process; 5−7 μm thick sections from rat skin biopsies were used on silanized slides with 2 % 3-aminopropyltriethoxysilane in acetone. The sample corresponded to rat skin that had been affixed in 4 % formaldehyde in 0.075 M sodium phosphate buffer pH 7.4, decalcified and fixed in paraffin. The slides were dewaxed and rehydrated following the regular protocol of the histopathology laboratory of the Universidad de Talca. Finally, the skin biopsies were stained with hematoxylin, eosin, Masson's trichrome, and Giemsa.

2.11. Antibacterial activity

The protocols were carried out according to Rodríguez Nuñez et al. (2019). First, MWCNTsCCH-TS (50 mg) was disposed into a tube with 5 mL of PBS (pH 7.4) as a "release medium". Simultaneously, a tube with 5 mL of PBS loaded with 1 mg of antibiotic was prepared and used as a control. Second, tubes were transferred to an orbital shaker incubator water bath (Farazteb, Iran) at 37 ± 0.1 °C. At specific time intervals (depending on the assay), 200 μL of release medium was taken and replaced with an equal volume of PBS to maintain sink conditions throughout the study. Finally, the samples of each tube were analyzed by screening the antimicrobial activity and quantitatively testing the antibacterial activity, as depicted below.

2.11.1. Screening of antimicrobial activity of MWCNTsCCH-TS against E. faecium

To evaluate the inhibitory activity against *E. faecium*, a qualitative test with a ring-diffusion method was performed. To evaluate the antibacterial activity of the prepared formulation, the gram-positive strain *E. faecium* ATCC® 19,434 was used as a model pathogen. The bacteria were grown overnight in MRS broth at 37 °C. The inoculum (100 μL) containing *E. faecium* (adjusted to ~1.0×10^6 CFU mL^{-1}) was spread previously on the agar surface. Afterward, wells (8 mm in diameter) were made on an agar plate and filled with 100 μL of release medium (see Section 2.10) of the specific interval times (1, 3, 6, 24 and 48 h). Moreover, two internal controls were treated with linezolid (10 and 15 μg mL^{-1}). The plates were incubated at 37 °C for 24 h. Antibacterial activity was estimated by the formation of bacterial inhibition zones surrounding the film disks. All screening assays were carried out in duplicate.

2.11.2. Quantitative test of the antibacterial activity of MWCNTsCCH-TS against E. faecium

For this assay, *E. faecium* ATCC® 19434 in the concentration range of 1.0×10^6 CFU mL^{-1} was inoculated in 1 mL of LB broth at 37 °C until reaching turbidity equivalent to that of a 0.5 McFarland standard. Next, 150 μL of release medium (from sample and control) with specific interval times (1, 2, 6, 24, 48 and 72 h) was added to 2 mL of the previous inoculation solution and then shaken at 200 rpm for 24 h at 37 °C. Afterward, each culture was tested; serial dilutions were performed in 0.1 % sterile peptone water. From each of these dilutions, 100 μL aliquots were obtained, which were plated on plate count agar and incubated at 37 °C for 24 h. Then, viable cell counts were carried out. All trials were performed in triplicate.

2.12. Cytotoxicity and cell viability

CNTs-CCH cytotoxicity was assessed in fibroblast cells. For this aim, fibroblast biocompatibility was studied through the MTT assay according to the method of Mosmann (1983). Briefly, fibroblasts were seeded in 24-well plates (5 μL, 1.6×10^4 cells per well), and 150 μL of Dulbecco's modified Eagle's medium (DMEM)-high glucose medium was added and incubated for 24 h at 37 °C in 5 % CO_2. Next, the medium was replaced by 100 μL of new DMEM-high glucose per well containing three different concentrations of MWCNTsCCH-TS (500 μg mL^{-1}, 1500 μg mL^{-1}, and 2500 μg mL^{-1}). A new medium without MWCNTsCCH-TS was utilized as a control. Cell viability was analyzed after 24 h by MTT tests. Specifically, 5 μL of MTT solution (3 mg mL^{-1} in PBS) and 50 μL of new medium were added to each sample and incubated for 4 h at 37 °C in the dark; formazan crystals were then dissolved in 100 μL of dimethyl sulfoxide (DMSO) and incubated for 18 h. The supernatant was analyzed at 570 nm (Spectrophotometer, Packard Bell, Meriden, CT, USA). Untreated cells were referenced as controls with 100 % viability. Finally, the cytotoxicity of MWCNTsCCH-TS on fibroblast cells was expressed as the relative viability (%), which correlates with the number of viable cells compared with the negative cell control (100 %).

2.13. Statistical analysis

All experiments were carried out in triplicate. The mean, standard deviation and Student's *t*-test were calculated to determine the statistical significance in several experiments such as ESR analysis, cumulative release test, quantitative test of antibacterial activity, and MTT assay. Graphs of the study results were designed by utilizing GraphPad Prism 6. Statistical significance was set at $p < 0.05$.

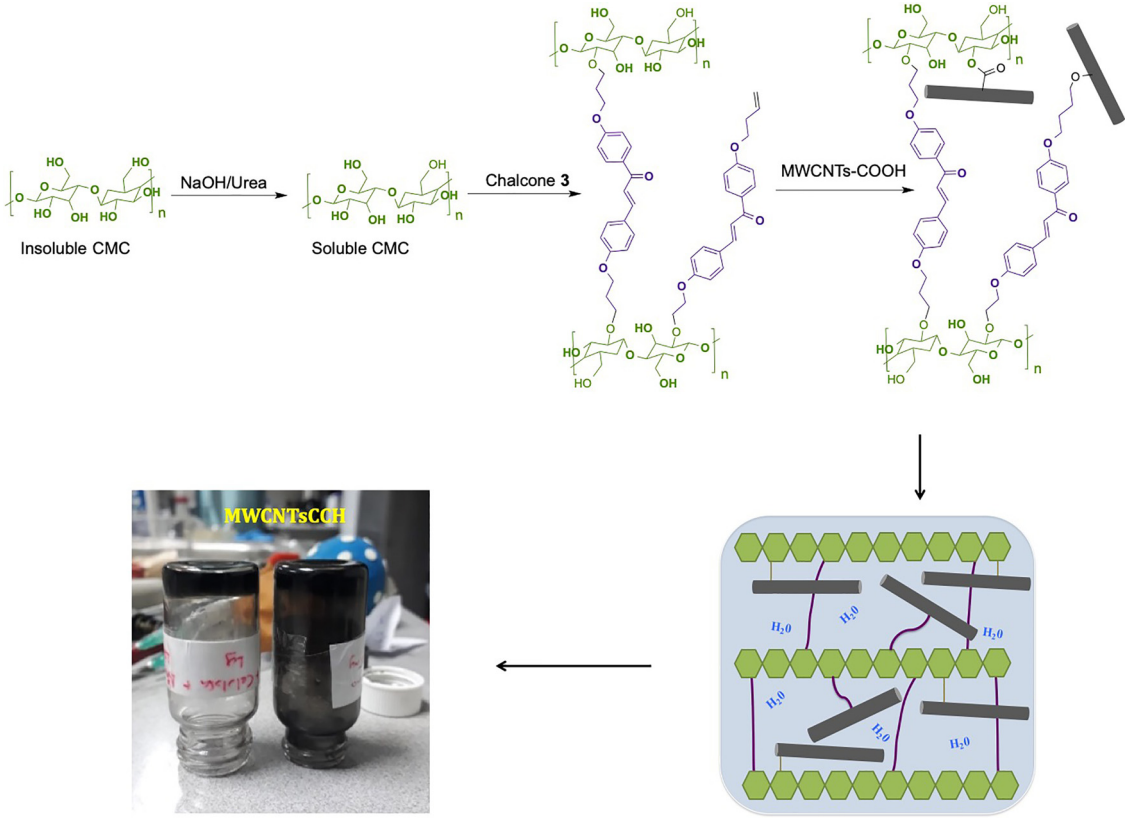

Fig. 1. Proposed structures of MWCNTsCCH.

3. Results

3.1. Synthesis of MWCNTsCCH-TS

The MWCNTsCCH-TS preparation was performed as depicted in Fig. 1. The synthesis of this hydrogel was conducted in a sequence of four successive steps. A NaOH/urea solution was used to solubilize cellulose with the goal of breaking the intermolecular hydrogen bonds of polysaccharides (a physical process) (Zhou & Zhang, 2000). Then, CH was added to the cellulose solution as a crosslinker agent, resulting in a prehydrogel solution. As in previous works, a crosslinking degree of 20 % was prepared with CH owing to its excellent features such as porosity, among others (Marican et al., 2018; Rodríguez Nuñez et al., 2019). Subsequently, to the prehydrogel solution, a specific amount of MWCNTs-COOH was added to obtain a homogenized black mixture (black prehydrogel)). Finally, the black prehydrogel was placed in an oven to complete hydrogel film formation (see Fig. 1). The MWCNTs-CH-cellulose hydrogel formation was evident based on the IR, TG-DTG and SEM analyses (see the next sections).

To prepare TS-loaded MWCNTsCCH (MWCNTsCCH-TS), a black prehydrogel solution was used, and a specific amount of TSs was added, as depicted in Table S1. With the cargo loading methodology performed, the TSs and prehydrogel became mixed, and it was possible to obtain over 98 % retention of each drug (Ávila-Salas et al., 2019).

3.2. ESR

This simple characterization allows us to confirm hydrogel network formation before any other analysis. Considering that it is desirable to study the release of bioactive compounds under physiological pH conditions, the ESR was evaluated at pH values of 7.4 and 4.0. As depicted in Fig. S3, an increase in the swelling index of MWCNTsCCH over time was observed at both pH values. The swelling index in the first section increased quickly and then gradually. This behavior may be due to the hydrogel reaching maximum constant swelling. The MWCNTsCCH reached swelling equilibrium (zero order) at approximately 8 h. After 8 h, the formulation reached approximately 170 % of the swelling index at pH 7.4. By contrast, at pH 4.0, 115 % of the swelling index was reached. The ESR difference at the two pH values is due to the protonation degree of the carboxylic acid-free MWCNTs.

3.3. Fourier transform infrared (FT-IR) spectroscopy analysis

To verify formation of the supramolecular complex hydrogel, FT-IR measurements of lyophilized MWCNTsCCH were performed; the results are shown in Fig. 2. The IR spectrum of MWCNTs-COOH shows important absorption bands at 3437 cm^{-1} (attributed to OH stretching vibrations), a very small intensity of two bands at 2920 and 2960 characteristic of –CH2 asymmetric and symmetric stretching vibrations, respectively, a band at 1636 cm^{-1} (assigned to conjugated CC stretching vibrations) and aliphatic hydroxyl bending vibrations (1438 $cm^{-}=^{1}$). Additionally, a small intensity band at 1701 cm^{-1} can be assigned to stretching vibrations of carbonyl groups (CO═) present in carboxylic acids (RCOOH) (Avilés, Cauich-Rodríguez, Moo-Tah, May-Pat, & Vargas-Coronado, 2009). In addition, in the IR spectrum of cellulose, two bands at 3345 and 1065 cm^{-1} characteristic of OH and a COC −−−−−tension band are observed; along with these bands, signals at 2900 (−CH), 1438 ($CH-_2$) and 1378 ($CH-_3$) cm^{-1} are also noted (Kim, Jeong, Park, Yu, & Jung, 2018). Additionally, the IR spectrum of CNTs-CCH was obtained. The most notable evidence of MWCNT functionalization was the increased intensity and shift of the carbonyl functional group stretching band. In the IR spectra of the MWCNTs-CH-cellulose hydrogel, stretching bands at 1664 (R-CO-OR) and 1071 (−COC) $cm^{-}---^{1}$ are observed, as shown in Fig. 2, providing evidence of ester-type bonds present in the MWCNTs-CH-cellulose hydrogel; additionally, the intense band at 1600 cm^{-1} corresponding to

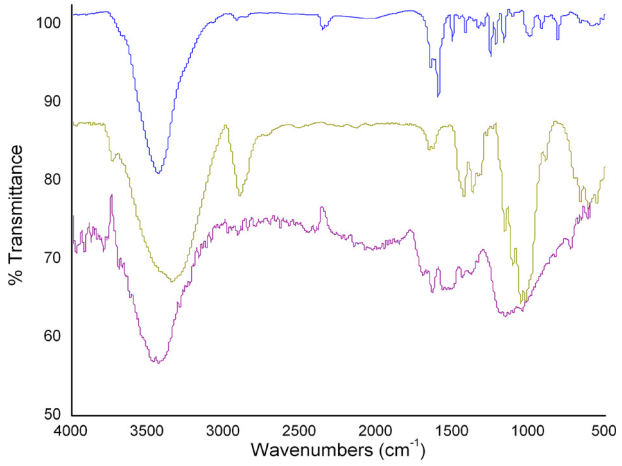

Fig. 2. IR spectra of MWCNTsCCH. Cellulose: olive-green line, oxidized MWCNTs: purple line and MWCNTsCCH with CH as a crosslinker agent (blue line).

(α, β-unsaturated) CO═ groups from the CH moiety is observed. On the other hand, a large band between 3600 and 3200 cm^{-1} is detected, which can be attributed to the OH− bonds of cellulose; moreover, it is possible to observe a very small band at ≈ 1739 cm^{-1} ascribed to acidic carbonyl groups, demonstrating that MWCNTs-COOH, which do not covalently bond to the crosslinker or cellulose, are present in the prepared hydrogel (Oishi, Nakaya, Matsui, & Hotta, 2015; Zhang, Zhang, Lu, & Liang, 2013). Therefore, these IR signals give solid evidence of MWCNTs-CH-cellulose hydrogel formation.

3.4. Thermogravimetric analysis

The mass loss (TG) and derivative (DTG) curves were obtained in the interval of room temperature to 800 °C. The thermal oxidative decomposition processes occurred as several consecutive and simultaneous steps of mass loss, mainly three and five steps. The first step of thermal decomposition (I) (Table S2) for MWCNTs-COOH was observed at 30 − 169 °C, with a total mass loss of 29.0 %, which was mainly attributed to the removal of moisture and degradation of C−OOH groups. Abuilaiwi and coworkers reported an initial decomposition temperature of 170 °C, with a maximum mass loss of the acidic −COOH groups at approximately 321 °C and completion of the degradation at approximately 480 °C (Abuilaiwi, Laoui, Al-Harthi, & Atieh, 2010). Our results follow the same trend (step II, 169 − 302 °C; 46.9 %). Additionally, MWCNTs-COOH exhibit a step of degradation at approximately 783 °C, corresponding to the oxidation of MWCNTs due to decomposition of the carboxylic groups, releasing oxygen into the chamber of the TG system. The CNTs-CCH have better thermal behavior than MWCNTs-COOH, and the formulation showed four degradation steps, with a 74.2 % global mass loss. CH showed four degradation steps and a 74.2 % global mass loss. Degradation step I of the formulation is attributed to water loss, while step II provides more information on the covalent ester bonds between MWCNTs-COOH, CH and cellulose. The Tm/°C value of the hydrogel is 211 °C, showing excellent thermal behavior. On the other hand, the temperature range 220 − 315 °C (Tm/°C of ≈ 268 °C) in steps II and III of the MWCNTs-CH-cellulose hydrogel gives us information about cellulose degradation in relation to the remaining hemicellulose, which required more energy for its degradation in the MWCNTs-CH-cellulose hydrogel (Tm/°C; 301) and represented 62.6 % of the mass loss (Yang, Yan, Chen, Lee, & Zheng, 2007). On the other hand, the temperature range is 315 − 400 °C with a Tm/°C of ≈ 355, which corresponds to cellulose pyrolysis, with the CH crosslinker being more stable (Tm/°C; 439) (Yang et al., 2007), suggesting a successful chemical crosslinking process by CH in MWCNTs-CH-cellulose hydrogel formation (Fig. 3). The TG-DTG analysis results were consistent with the FT-IR spectra.

3.5. SEM analysis: viewing

The results from the SEM investigation of MWCNTsCCH are depicted in Fig. 4. For MWCNTsCCH (see Fig. 4a), a compact and disorganized structure was observed. Some pores were detected in the hydrogel. It appears that the film morphology was influenced by the crosslinker chemical structure. Additionally, in some zones of the sample surface, various nanotubes were identified. In Fig. 4b, the prepared MWCNTs are observed to exhibit their typical morphology.

3.6. In vitro release behavior of TSs by supramolecular MWCNTsCCH-TS

The TS release evaluation was carried out with a 400 mg film charged with allantoin, dexpanthenol, resveratrol, and linezolid. The encapsulation procedure was performed through a simple route as described previously by Ávila-Salas et al. (2019). Briefly, the encapsulation process was carried out by mixing the therapeutic substances (at specific concentrations) with the prehydrogel solution. Finally, the supramolecular complex MWCNTsCCH-TS was obtained. As an advantage, this method permitted the loading of an exact amount of drugs. Therefore, for each film dressing applied, there is 13.6 mg of allantoin and 5.5 mg each of dexpanthenol, resveratrol, and linezolid according to the standard concentrations of bioactive compounds applied in dermatology.

To analyze the *in vitro* kinetic release of TSs from MWCNTsCCH-TS, these profiles were obtained under physiological conditions (33.5 °C, PBS at pH 7.4). The samples were assessed by HPLC. The cumulative released percent of each bioactive compound was monitored over time. These results are presented in Fig. 5. MWCNTsCCH-TS offered a rapid release into the medium until 12 h for all TSs. By 12 h, 30 % linezolid, 44 % allantoin, 56 % dexpanthenol and 61 % resveratrol had been released from MWCNTsCCH-TS. After this initial fast release profile, MWCNTsCCH-TS exhibited a slower and continuous TS release into the medium. The average rapid-release phase was 0.4 mg/h, 0.5 mg/h, 0.6 mg/h and 1.2 mg/h for allantoin, dexpanthenol, resveratrol and linezolid, respectively. This rate changed after 12 h, and the average of the slow-release phase was 0.17 mg/h, 0.14 mg/h, 0.15 mg/h and 0.11 mg/h for allantoin, dexpanthenol, resveratrol, and linezolid, respectively. In Table 1, all the average release values of each TS are shown. The release patterns of the formulation are dependent on each TS, its structure, and intermolecular interactions with the matrix of the hydrogel (Shekunov, Chattopadhyay, Tong, Chow, & Grossmann, 2007). According to the release rate, the order is resveratrol > dexpanthenol > allantoin > linezolid, as shown in Fig. 5. The obtained results are interesting from the point of view of coordinated healing action, in which the first release (higher release) is of resveratrol. This finding implies that the compound could act at the first stage of healing as a radical scavenger and affect hemostasis and inflammation (Liu et al., 2015). Subsequently, dexpanthenol and allantoin are released, whose action is on proliferation and remodeling (Sowa et al., 2018, Durmus et al., 2012; Heise et al., 2012). Finally, linezolid was released at a relatively slower rate, and this result is interesting from point of view of the drug having more efficient antimicrobial action at constant, low doses, enabling high-efficiency therapy and avoiding more antibiotic resistance by *E. faecium*.

To elucidate the mechanism of TS release, the obtained averages of the release profiles were fitted through mathematical models. The coefficients of correlation (r) and release exponent (n) are shown in Table S3 of the supporting information. The results revealed that for the coefficients of correlation (r), among all the studied models, the Korsmeyer–Peppas model was the best fit for the formulation. The *n* values (between 0.33954 and 0.43296 for all TSs) suggested that the mechanism for TS release was pseudo-Fickian.

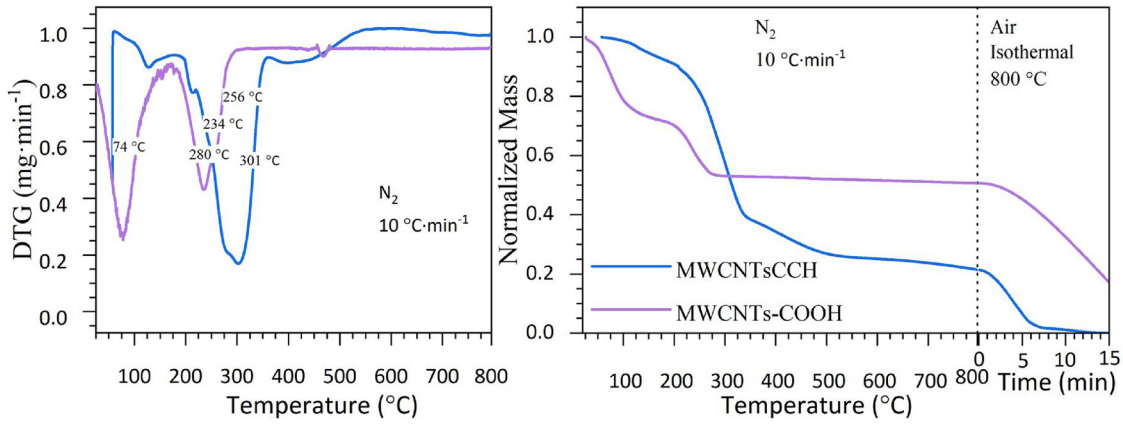

Fig. 3. TG and DTG analysis of MWCNTsCCH in nitrogen and air as reactive gas.

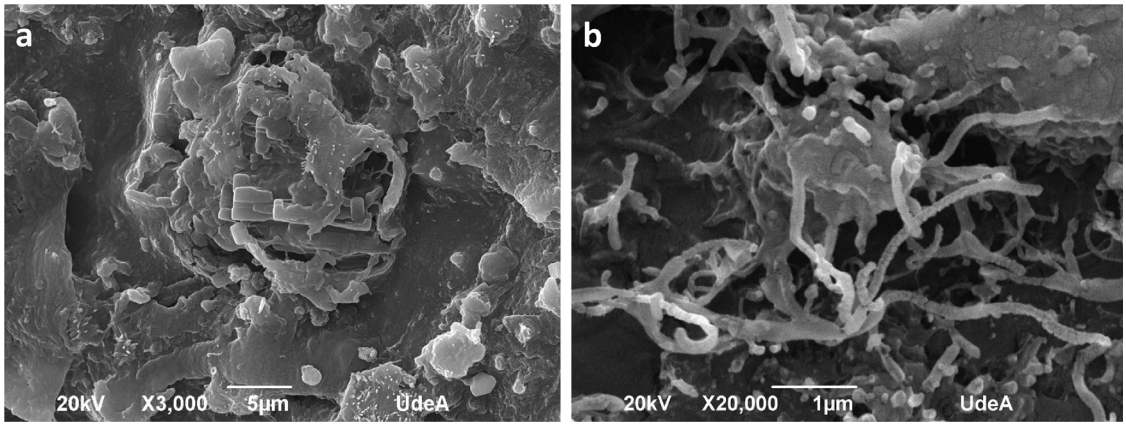

Fig. 4. SEM micrographs of MWCNTsCCH (a) and MWCNTs (b).

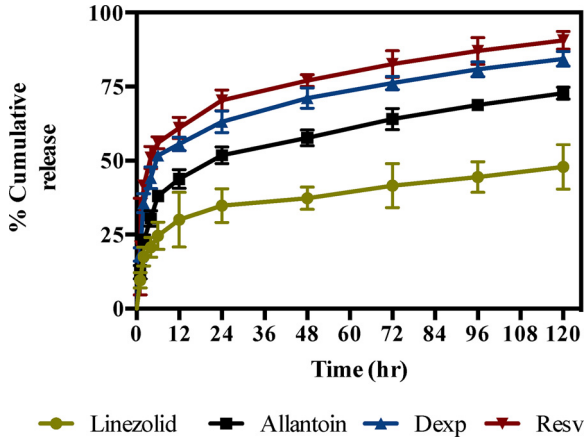

Fig. 5. Release of TSs from MWCNTsCCH-TS in PBS at 33.5 °C; mean ± SEM, n = 3.

3.7. *In vitro* wound scratch characterizations

To investigate the wound healing efficacy of MWCNTsCCH-TS, an *in vitro* scratch-wound recovery assay was performed. In this context, for skin wound healing, cell migration is essential for wound contraction and the later healing stages. Fig. 6a depicts the scratch assay results (photograph) utilizing the L929 dermal fibroblast cell line to calculate the *in vitro* wound closure effects of the MWCNTsCCH-TS groups. Fig. 6b shows the percentage of wound healing closure at 24 and 48 h. At 24 h, the wound closure process was only observed in the MWCNTsCCH-TS and commercial product groups (44 and 17 %, respectively). In contrast, in the negative control and the MWCNTsCCH groups, the signal of wound healing was not detected. At 48 h, almost complete wound closure of the scratches in the MWCNTsCCH-TS group was observed in L929 cultures (94 %) compared with the results in the negative control (20 %), MWCNTsCCH (11 %), and commercial product (57 %) groups. MWCNTsCCH-TS significantly improved the rate of wound closure at both 24 and 48 h in the L929 fibroblast cell line.

Table 1
Release profile of MWCNTsCCH-TS.

			Release profile			
			Allantoin	Dexpanthenol	Resveratrol	Linezolid
Release phase	Rapid*	% Released	51,8 ± 2	63,1 ± 1,8	70,3 ± 1,7	34,8 ± 1,2
		Release rate (mg/h)	0,4 ± 0,01	0,5 ± 0,02	0,6 ± 0,02	1,2 ± 0,05
	Slow**	% Released	48,2 ± 1,9	36,9 ± 1,6	29,7 ± 1,4	65,2 ± 3,2
		Release rate (mg/h)	0,11 ± 0, 004	0,16 ± 0, 008	0,14 ± 0,005	0,15 ± 0, 005

(*) The rapid phase occurred during 24 h. (**) The release rate was calculated in a specific time frame because until 120 h, the formulation still released TSs.

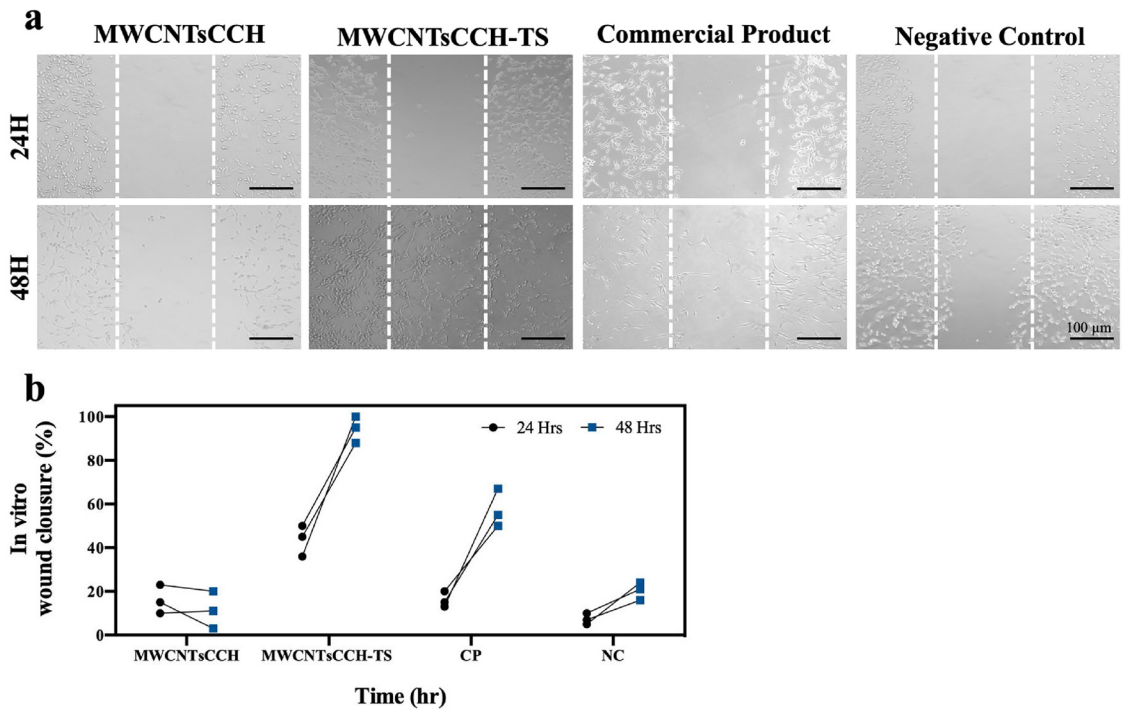

Fig. 6. *In vitro* scratch assays (a) and percentage wound closure (b).

3.8. *In vivo wound closure studies and histological analysis*

Fig. 7 depicts the images of the skin wound taken on day 0 and day 14 after treatment with MWCNTsCCH-TS and controls. After the 14th day, the wounds treated with MWCNTsCCH-TS showed promising results compared with the controls.

The fundamental characteristic detected was the growth of the new epidermis, which was reduced towards the wound center in treated wound lesions, resulting in a reduced wound area. For instance, MWCNTsCCH-TS achieved complete healing, while NC and CP had wound healing ratios of 40 and 85 %, respectively. The wound healing effect of MWCNTsCCH-TS could be due to the synergistic effects among the therapeutic substances and their organized sustained release over the wound area. Consequently, treatment with MWCNTsCCH-TS led to enhanced wound healing efficacy. Theoretical and experimentally, it was demonstrated that the proposed combinatorial therapy may represent a new advance in wound healing rehabilitation.

Wound healing is an intricate process that involves the following overlapping but well-defined stages: hemostasis, inflammation, migration, proliferation, and remodeling (Ávila-Salas et al., 2019). Hematoxylin and eosin (H&E), Masson's trichrome and Giemsa staining were used to assess wound healing progress. The histology investigation of wounds covered with MWCNTsCCH-TS and controls on the 14th postoperative day is displayed in Fig. 8.

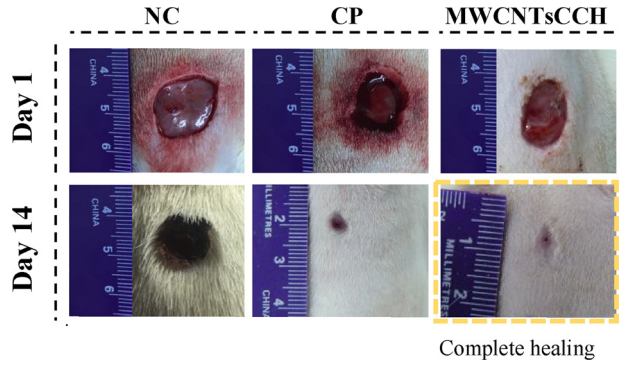

Fig. 7. *In vivo* evaluations of MWCNTsCCH-TS for wound healing (wound closure). NC: MWCNTsCCH (negative control, film dressing without TSs); CP: Madecassol™ (commercial product); MWCNTsCCH-TS as the proposed film dressing.

In the negative control (see Fig. 8a), the histological assessment reveals a limited organization of the area under repair. Thin, stratified keratinized epithelium was observed. Moreover, the nonexistence of re-epithelialization was detected. No structural epithelium organization was perceived, nor was an increase in the content of cellular components such as fibroblasts, inflammatory cell and endothelial cells detected, representing a poor organization of the connective tissue. In the central zone, some angiogenic processes were observed. On the other hand, modest hemorrhaging consisting of extravasated red blood cells towards the deep area was detected. Finally, some emerging hair follicles at the edges of the healing area were identified.

Compared with the results of the negative control (see Fig. 8c), lining epithelium that covers the entire zone of repair is detected, which represents a total re-epithelialization and advanced level of the repair process. Moreover, in the connective tissue, organized collagen was detected in the peripheral zone of the repair zone. Furthermore, fibrous tissue in the deep area of the sample was observed. This tissue is associated with skeletal muscle tissue, suggesting a high level of organization in the wound healing process.

Regarding the commercial product (see Fig. 8b), results similar to those with MWCNTsCCH-TS were obtained; however, this formulation was applied daily for 14 days, unlike the prepared formulation that was applied only once.

These findings are consistent with the closure and scratch assay (see Figs. 6 and 7), in which MWCNTsCCH-TS presented wound closure close to 100%. Additionally, these results could be correlated with the *in vitro* release profile of MWCNTsCCH-TS (Fig. 5), in which resveratrol and dexpanthenol were released first (anti-inflammatory activity and proliferation-stimulating activity, respectively). Later, allantoin and linezolid were released (proliferation-stimulating activity and antibacterial activity, respectively). It is interesting to note that the TS release order is adjusted to the wound healing stages.

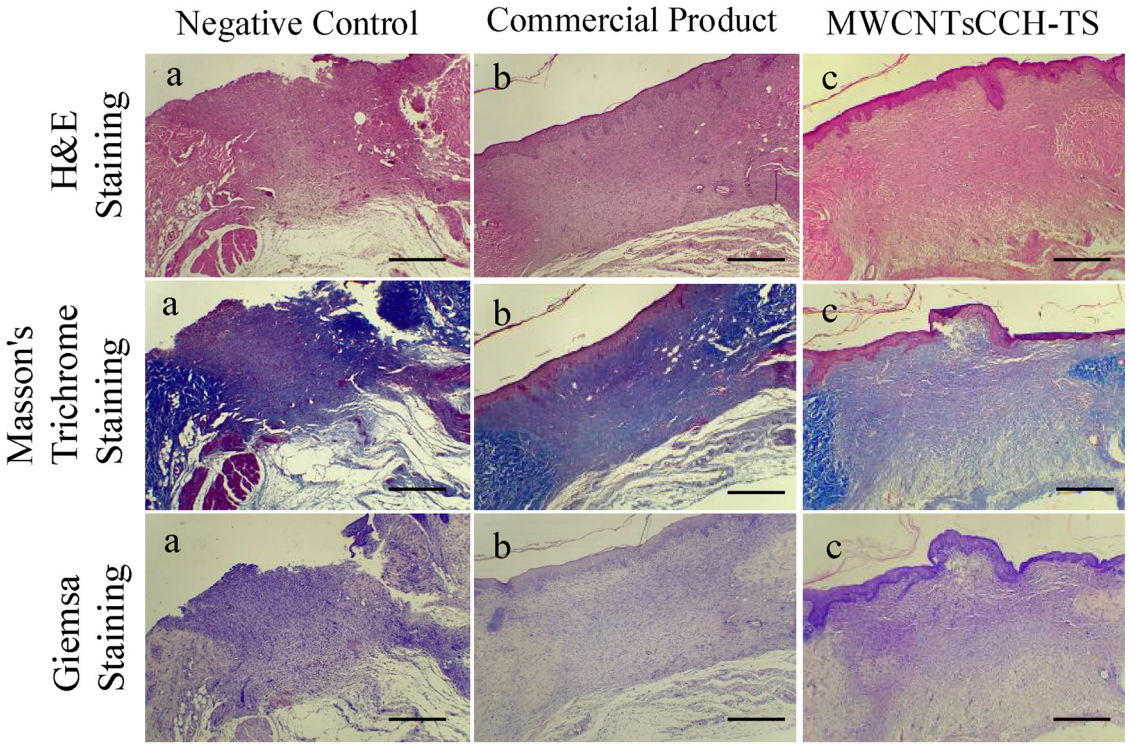

Fig. 8. Histological images of H&E-, Masson's trichrome- and GIEMSA-stained sections after 14 days of wound healing. Negative Control: MWCNTsCCH; Commercial Product: Madecassol® and MWCNTsCCH-TS (prepared formulation) Scale bars are 100 μm.

3.9. Antibacterial studies

Recent studies suggest that the antibacterial activity of antibiotics can be improved through sustained release. Moreover, this approach could involve a lower probability of triggering bacterial resistance (Canaparo et al., 2019; Gao, Nie, Zou, Shi, & Cheng, 2011). Consistent with the above consideration, the results of this work, summarized in Fig. 9, indicate that the linezolid action is more effective over time than the control (in the control, the antibiotic doses were delivered directly in the supernatant). Here, we can conclude that sustained release at constant doses in the supernatant from the prepared hydrogel could maintain the antibiotic integrity with better activity over time, as shown in Fig. 9b. In contrast, in the control, the antibiotic had a better effect in the first hour; however, it lost effectiveness over time, as depicted in Fig. 9a. Fig. 9c displays the screening of the antimicrobial activity of MWCNTsCCH-TS and the control. The inhibition zone of *E. faecium* of each aliquot was recorded at certain times up to 48 h. The inhibition zone of the control in the first hour was greater than ~30 mm; however, over time, the zone size decreased, reaching ~20 mm at 48 h. In the prepared formulation case, the inhibition zone was initially ~23 mm, increasing in size during the subsequent hours to ~28 mm and finishing at 30 mm after 48 h. These results support the quantitative findings of antibacterial activity against *E. faecium*, as demonstrated in Fig. 9d. Under the same methodology of obtaining samples as in the previous experiment, the release medium with linezolid was placed in a solution with *E. faecium*. Here, the results showed that the control increased the UFC of bacteria over time, indicating that linezolid lost its activity after 72 h. In contrast, the assays with the release medium from the prepared formulation maintained the UFC during the time, thereby indicating that linezolid acted as a bacteriostatic agent. Two additional experiments were performed with MWCNTsCCH and MWCNTsCCH-TS without linezolid. Nevertheless, the antibacterial activity in both cases was not significant (data not shown).

3.10. Viability studies of MWCNTsCCH

This experiment was carried out to measure fibroblast cell viability after exposure to MWCNTsCCH. The biocompatibility of sterilized MWCNTsCCH after 24 h was evaluated by a cell viability assay using L929 fibroblast cells. Fig. S4 shows the fibroblast cell viability in the presence of three different concentrations of MWCNTsCCH (500, 1500 and 2500 μg mL^{-1}). As specified in Fig. S4, at 500 μg mL^{-1}, the cell viability was near 100 %. Furthermore, it was observed that when considerably increasing the MWCNTsCCH concentration, the fibroblast cell viability only decreased vaguely. This result means that at 1500 and 2500 μg mL^{-1}, the cell viability decreases by 95 and 89 %, respectively. These results corroborate that MWCNTsCCH has an almost nonexistent effect on fibroblast cells. These executed analyses allow us to conclude that MWCNTsCCH could be biocompatible for medical purposes. Thus, MWCNTsCCH could be considered an innocuous formulation for the sustained release of therapeutic agents involved in chronic wound healing.

4. Conclusion

A multifaceted formulation based on a carbon nanotube-containing cellulose-chalcone hydrogel with sustained release of therapeutic substances exhibiting wound healing and antibacterial properties was successfully prepared. The hydrogel was prepared by crosslinking cellulose and substituted chalcone. Moreover, the formulation was conjugated with multiwalled carbon nanotubes with the aim of improving the loading of the bioactive compounds allantoin, dexpanthenol, resveratrol, and linezolid. In the present work, allantoin has been studied owing to its numerous pharmacological activities mainly related to wound healing. Resveratrol and dexpanthenol were studied as well because they have been reported to exhibit anti-inflammatory activity and promote wound healing. On the other hand, linezolid was included in this report because it is an antibiotic that is effective in treating skin and soft tissue infections, principally infections triggered by antibiotic-

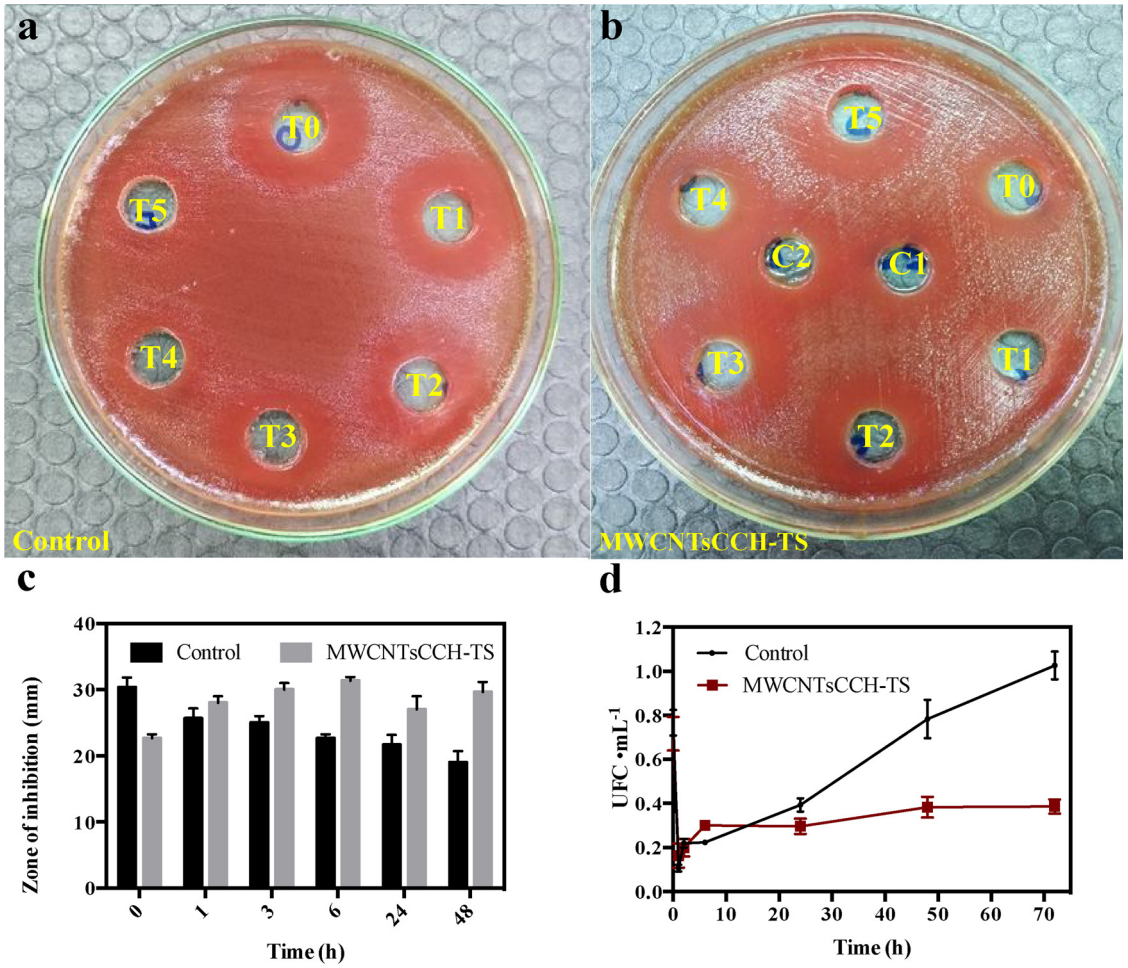

Fig. 9. Screening of the antibacterial effect of MWCNTsCCH-TS. Control (a); MWCNTsCCH-TS (b); T0: 0 h, T1: 1 h, T2: 3 h, T3: 6 h, T4: 24 h, T5: 48 h; the antibacterial effect was expressed as the inhibition area against *E. faecium* (c); Quantitative test of antibacterial activity against *E. faecium* (d). (*) C1 and C2 in Fig. 9b are positive controls of 10 and 15 μg mL^{-1} linezolid, respectively.

resistant bacteria.

Taken together, the swelling response, FT-IR, TG-DTG, and SEM results corroborate the formation of the MWCNTs-CH-cellulose hydrogel. The swelling index results indicated that MWCNTsCCH is stimuli-responsive to pH. The prepared hydrogel showed a sustained release rate of therapeutic substances according to the results shown in the chromatographic studies. From these results, it is possible to carry out a combinatorial and coordinated sustained release of all four bioactive compounds, indicating that this approach could be an efficient strategy to achieve wound healing. The prepared hydrogel and its efficiency in the controlled release of the four compounds can be attributed to several physicochemical characteristics of the hydrogel such as the specific matrix crosslinking degree, functional groups (alcohols and amines), and less polar components (carbon nanotubes). The supramolecular complex designed with different components allows sustained release of each compound based on their affinities, polarities, and sizes. The drug release profile of MWCNTsCCH was found to follow the Korsmeyer-Peppas release model, and the release mechanism for the TSs was pseudo-Fickian.

The above outcomes were confirmed by *in vitro* wound closure and *in vivo* wound healing studies that showed an improved wound healing process in a full-thickness skin defect model. The TSs allantoin, dexpanthenol, resveratrol, and linezolid displayed some differences regarding the release rate, which seemed to be governed by the affinity of each bioactive compound type and the hydrogel pores in the matrix (intermolecular interactions).

Macroscopically, wound lesions treated with MWCNTsCCH-TS exhibited growth of the new epidermis towards the wound center, resulting in reduced wound areas. The microscopic evidence suggests that the histology of the wound healing process is consistent with the scratch assay and wound closure results.

On the other hand, the antibacterial assays demonstrated that the sustained release of linezolid tends to be very effective when its bioavailability is dosed periodically. This assessment also presumes that the antibiotic remained more bioactive when released from the hydrogel than when conventionally released by the control (antibiotic delivered directly). This finding could suggest that the hydrogel has the capability to protect the antibiotic from degradation.

MWCNTsCCH showed good biocompatibility with L929 mouse connective tissue fibroblasts. The results exhibited cell viability exceeding 95 %. In conclusion, a multifaceted hydrogel-based formulation could potentially be utilized in complex wounds to improve wound healing and to prevent potential infectious processes.

CRediT authorship contribution statement

Oscar Forero-Doria: Investigation, Data curation, Formal analysis. **Efrain Polo:** Investigation, Methodology, Visualization. **Adolfo Marican:** Conceptualization, Data curation, Formal analysis. **Luis Guzmán:** Conceptualization, Validation. **Bernardo Venegas:** Methodology. **Sekar Vijayakumar:** Methodology, Writing - review & editing. **Sergio Wehinger:** Visualization, Supervision. **Marcelo**

Guerrero: Methodology, Data curation. **Jaime Gallego:** Formal analysis. **Esteban F. Durán-Lara:** Conceptualization, Resources, Writing - original draft, Supervision, Project administration, Funding acquisition.

Declaration of Competing Interest

There are no conflicts to declare.

Acknowledgments

This work was supported by FONDECYT (Chile) through project Nº 11170155 from Esteban F Durán-Lara. Oscar Forero-Doria thanks FONDECYT (Post-Doctoral Fellowship No. 3170757).

References

Abuilaiwi, F., Laoui, T., Al-Harthi, M., & Atieh, M. A. (2010). Modification and Functionalization of Multiwalled Carbon Nanotube (MWCNT) via FISCHER Esterification. *Arabian Journal for Science and Engineering, 35*, 37–48.

Adesida, S. A., Ezenta, C. C., Adagbada, A. O., Aladesokan, A. A., & Coker, A. O. (2017). Carriage of multidrug resistant *Enterococcus faecium* and *Enterococcus faecalis* among apparently healthy humans. *African Journal of Infectious Diseases, 11*(2), 83–89.

Alavi, M. (2019). Modifications of microcrystalline cellulose (MCC), nanofibrillated cellulose (NFC), and nanocrystalline cellulose (NCC) for antimicrobial and wound healing applications. *e-Polymers, 19*, 103–119.

Ávila-Salas, F., Marican, A., Pinochet, S., Carreño, G., Valdés, O., Venegas, B., et al. (2019). Film dressings based on hydrogels: Simultaneous and sustained-release of bioactive compounds with wound healing properties. *Pharmaceutics, 11*(9), 447.

Avilés, F., Cauich-Rodríguez, J. V., Moo-Tah, L., May-Pat, A., & Vargas-Coronado, R. (2009). Evaluation of mild acid oxidation treatments for MWCNT functionalization. *Carbon, 47*(13), 2970–2975.

Bertsch, P., Schneider, L., Bovone, G., Tibbitt, M. W., Fischer, P., & Gstöhl, S. (2019). Injectable biocompatible hydrogels from cellulose nanocrystals for locally targeted sustained drug release. *ACS Applied Materials & Interfaces, 11*(42), 38578–38585.

Blacklow, S. O., Li, J., Freedman, B. R., Zeidi, M., Chen, C., & Mooney, D. J. (2019). Bioinspired mechanically active adhesive dressings to accelerate wound closure. *Science Advances, 5*(7), eaaw3963.

Bottini, M., Bruckner, S., Nika, K., Bottini, N., Bellucci, S., Magrini, A., et al. (2006). Multi-walled carbon nanotubes induce T lymphocyte apoptosis. *Toxicology Letters, 160*(2), 121–126.

Canaparo, R., Foglietta, F., Giuntini, F., Della Pepa, C., Dosio, F., & Serpe, L. (2019). Recent developments in antibacterial therapy: Focus on stimuli-responsive drug-delivery systems and therapeutic nanoparticles. *Molecules, 24*(10), 1991.

Capanema, N. S. V., Mansur, A. A. P., Carvalho, S. M., Carvalho, I. C., Chagas, P., de Oliveira, L. C. A., et al. (2018). Bioengineered carboxymethyl cellulose-doxorubicin prodrug hydrogels for topical chemotherapy of melanoma skin cancer. *Carbohydrate Polymers, 195*, 401–412.

Cass, P., Knower, W., Pereeia, E., Holmes, N. P., & Hughes, T. (2010). Preparation of hydrogels via ultrasonic polymerization. *Ultrasonics Sonochemistry, 17*(2), 326–332.

Durmus, A., Yaman, M., & Can, H. (2012). Effects of extractum cepae, heparin, allantoin gel and silver sulfadiazine on burn wound healing: an experimental study in a rat model. *Veterinarni Medicina, 57*(6), 287–292.

Dwivedi, R., Singh, A. K., & Dhillon, A. (2017). pH-responsive drug release from dependal-M loaded polyacrylamide hydrogels. *Journal of Science Advanced Materials and Devices, 2*(1), 45–50.

Ebner, F., Heller, A., Rippke, F., & Tausch, I. (2002). Topical use of dexpanthenol in skin disorders. *American Journal of Clinical Dermatology, 3*(6), 427–433.

Fu, L., Qi, C., Ma, M., & Wan, P. (2019). Multifunctional cellulose-based hydrogels for biomedical applications. *Journal of Materials Chemistry B, 7*(10), 1541–1562.

Gao, P., Nie, X., Zou, M., Shi, Y., & Cheng, G. (2011). Recent advances in materials for extended-release antibiotic delivery system. *The Journal of Antibiotics, 64*(9), 625–634.

Grimmig, R., Babczyk, P., Gillemot, P., Schmitz, K., Schulze, M., & Tobiasch, E. (2019). Development and evaluation of a prototype scratch apparatus for wound assays adjustable to different forces and substrates. *Applied Sciences, 9*, 4414.

Heise, R., Skazik, C., Marquardt, Y., Czaja, K., Sebastian, K., Kurschat, P., et al. (2012). Dexpanthenol modulates gene expression in skin wound healing in vivo. *Skin Pharmacology and Physiology, 25*(5), 241–248.

Herlem, G., Picaud, F., Girardet, C., Micheau, O., Mohapatra, S. S., Ranjan, S., et al. (2019). *Chapter 16 - Carbon nanotubes: Synthesis, characterization, and applications in drug-delivery systems. Nanocarriers for drug delivery*. Elsevier469–529.

Hickey, R., & Pelling, A. (2019). Cellulose biomaterials for tissue engineering. *Frontiers in Bioengineering and Biotechnology, 7*, 45.

Kabir, S. M. F., Sikdar, P. P., Haque, B., Bhuiyan, M. A. R., Ali, A., & Islam, M. N. (2018). Cellulose-based hydrogel materials: Chemistry, properties and their prospective applications. *Progress in Biomaterials, 7*(3), 153–174.

Kim, Y., Jeong, D., Park, K. H., Yu, J. H., & Jung, S. (2018). Efficient adsorption on benzoyl and stearoyl cellulose to remove phenanthrene and pyrene from aqueous solution. *Polymers, 10*(9), 1042.

Lebreton, F., van Schaik, W., McGuire, A. M., Godfrey, P., Griggs, A., Mazumdar, V., et al. (2013). Emergence of epidemic multidrug-resistant *Enterococcus faecium* from animal and commensal strains. *mBio, 4*(4), e00534–13.

Lin, X., Han, X., & Wang, J. (2018). In situ synthesis of easily separable Au nanoparticles catalysts based on cellulose hydrogels. *Polymer Journal, 50*, 495–501.

Liu, F. C., Tsai, Y. F., Tsai, H. I., & Yu, H. P. (2015). Anti-inflammatory and organ-protective effects of resveratrol in trauma-hemorrhagic injury. *Mediators of Inflammation, 2015*, 643763.

Marican, A., Ávila-Salas, F., Valdés, O., Wehinger, S., Villaseñor, J., Fuentealba, N., et al. (2018). Rational design, synthesis and evaluation of γ-CD-containing cross-linked polyvinyl alcohol hydrogel as a prednisone delivery platform. *Pharmaceutics, 10*(1), 30.

Mihai, M. M., Dima, M. B., Dima, B., & Holban, A. M. (2019). Nanomaterials for wound healing and infection control. *Materials (Basel), 12*(13), E2176.

Mir, M., Ali, M. N., Barakullah, A., Gulzar, A., Arshad, M., Fatima, S., et al. (2018). Synthetic polymeric biomaterials for wound healing: A review. *Progress in Biomaterials, 7*(1), 1–21.

Mohamad, N., Loh, E., Fauzi, M., Ng, M., & Amin, M. (2019). In vivo evaluation of bacterial cellulose/acrylic acid wound dressing hydrogel containing keratinocytes and fibroblasts for burn wounds. *Drug Delivery and Translational Research, 9*(2), 444–452.

Mosmann, T. (1983). Rapid colorimetric assay for cellular growth and survival: Application to proliferation and cytotoxicity assays. *Journal of Immunological Methods, 65*(1), 55–63.

Murray, R., West, Z., Cowin, A., & Farrugia, B. (2019). Development and use of biomaterials as wound healing therapies. *Burns & Trauma, 7*, 2.

Oishi, Y., Nakaya, M., Matsui, E., & Hotta, A. (2015). Structural and mechanical properties of cellulose composites made of isolated cellulose nanofibers and poly(vinyl alcohol). *Composites Part A, Applied Science and Manufacturing, 73*, 72–79.

Owonubi, S. J., Aderibigbe, B. A., Mukwevho, E., Sadiku, E. R., & Ray, S. S. (2018). Characterization and in vitro release kinetics of antimalarials from whey protein-based hydrogel biocomposites. *International Journal of Industrial Chemistry, 9*(1), 39–52.

Pan, Y., Zhao, X., Li, X., & Cai, P. (2019). Green-based antimicrobial hydrogels prepared from bagasse cellulose as 3D-Scaffolds for wound dressing. *Polymers, 11*(11), 1846.

Reiter, K. C., Villa, B., Paim, T. G., de Oliveira, C. F., & d'Azevedo, P. A. (2013). Inhibition of biofilm maturation by linezolid in meticillin-resistant *Staphylococcus epidermidis* clinical isolates: comparison with other drugs. *Journal of Medical Microbiology, 62*(3), 394–399.

Rodríguez Nuñez, Y. A., Castro, R. I., Arenas, F. A., López-Cabaña, Z. E., Carreño, G., Carrasco-Sánchez, V., et al. (2019). Preparation of hydrogel/silver nanohybrids mediated by tunable-size silver nanoparticles for potential antibacterial applications. *Polymers (Basel), 11*(4), 716.

Sefton, A. M. (2002). Mechanisms of antimicrobial resistance: Their clinical relevance in the new millennium. *Drugs, 62*(4), 557–566.

Shekunov, B. Y., Chattopadhyay, P., Tong, H. H., Chow, A. H., & Grossmann, J. G. (2007). Structure and drug release in a crosslinked poly(ethylene oxide) hydrogel. *Journal of Pharmaceutical Sciences, 96*(5), 1320–1330.

Smidt, E., Lechner, P., Schwanninger, M., Haberhauer, G., & Gerzabek, M. H. (2002). Characterization of waste organic matter by FT-IR spectroscopy: Application in waste science. *Applied Spectroscopy, 56*(9), 1170–1175.

Sowa, I., Paduch, R., Strzemski, M., Zielińska, S., Rydzik-Strzemska, E., Sawicki, J., et al. (2018). Proliferative and antioxidant activity of Symphytum officinale root extract. *Natural Product Research, 32*(5), 605–609.

Valdés, O., Ávila-Salas, F., Marican, A., Fuentealba, N., Villasenor, J., Arenas-Salinas, M., et al. (2018). Methamidophos removal from aqueous solutions using a super adsorbent based on crosslinked poly (vinyl alcohol) hydrogel. *Journal of Applied Polymer Science, 135*(11), 45964.

Ventola, C. L. (2015). The antibiotic resistance crisis: Part 1: Causes and threats. *Pharmacy and Therapeutics, 40*(4), 277–283.

Vijayakumar, S., Saravanakumar, K., Malaikozhundan, B., Divya, M., Vaseeharan, B., Durán-Lara, E. F., et al. (2019). Biopolymer K-carrageenan wrapped ZnO nanoparticles as drug delivery vehicles for anti MRSA therapy. *International Journal of Biological Macromolecules, 144*, 9–18.

Wang, F., Pan, Y., Cai, P., Guo, T., & Xiao, H. (2017). Single and binary adsorption of heavy metal ions from aqueous solutions using sugarcane cellulose-based adsorbent. *Bioresource Technology, 241*, 482–490.

Wu, J., Li, P., Dong, C., Jiang, H., Xue, B., Gao, X., et al. (2018). Rationally designed synthetic protein hydrogels with predictable mechanical properties. *Nature Communications, 9*(1), 620.

Yang, H., Yan, R., Chen, H., Lee, D. H., & Zheng, C. (2007). Characteristics of hemicellulose, cellulose and lignin pyrolysis. *Fuel, 86*, 1781–1788.

Ye, D., Zhong, Z., Xu, H., Chang, C., Yang, Z., Wang, Y., et al. (2016). Construction of cellulose/nanosilver sponge materials and their antibacterial activities for infected wounds healing. *Cellulose, 23*, 749–763.

Yue, J., Dong, B. R., Yang, M., Chen, X., Wu, T., & Liu, G. J. (2013). Linezolid versus vancomycin for skin and soft tissue infections. *The Cochrane Database of Systematic Reviews, 2013*(7), CD008056.

Zhang, L., Zhang, G., Lu, J., & Liang, H. (2013). Preparation and characterization of carboxymethyl cellulose/polyvinyl alcohol blend film as a potential coating material. *Polymer-Plastics Technology and Engineering, 52*(2), 163–167.

Zhou, J., & Zhang, L. (2000). Solubility of cellulose in NaOH/urea aqueous solution. *Polymer Journal, 32*, 866–870.